Electronic, Optical, and Magnetic Properties of $LiFePO_4$: Small Magnetic Polaron Effects

K. Zaghib,[†] A. Mauger,*[,‡] J. B. Goodenough,[§] F. Gendron,[||] and C. M. Julien[||]

Institut de Recherches d'Hydro-Québec, 1800 Boulevard Lionel-Boulet, Varennes, Québec, Canada J3X 1S1, Institut de Minéralogie et de Physique des Milieux Condensés, CNRS-UMR 7590, Université Pierre et Marie Curie, 140 rue de Lourmel, 75015 Paris, France, The University of Texas at Austin, 1 University Station, C2200, Austin, Texas 78712, and Institut des Nano-Sciences de Paris, CNRS-UMR 7588, Université Pierre et Marie Curie, 140 rue de Lourmel, 75015 Paris, France

Received April 16, 2007. Revised Manuscript Received May 25, 2007

The electronic structure of $LiFePO_4$ and delithiated $FePO_4$ is revisited in the light of the previous calculations taking into account the coulomb correlation potential for *d*-electrons. The nature of the optical transitions across the energy gap is investigated. In $LiFePO_4$, these are intra-atomic $Fe^{2+}-Fe^{3+}$ transitions suffering a strong Franck−Condon effect due to the local distortion of the lattice in $FePO_4$, which is indirect evidence of the formation of a small polaron. This situation contrasts with that met in the much more covalent delithiated phase, where the optical transition across the energy gap is associated with a transfer of an electron from the p-states of the oxygen to the d-states of iron ions. The small polarons in $LiFePO_4$ are associated with the presence of Fe^{3+} ions introduced by native defects in relative concentration $[Fe^{3+}]/[Fe^{2+}+Fe^{3+}] = 3 \times 10^{-3}$ in the samples known to be optimized with respect to their electrochemical properties. The nearest iron neighbors around the central polaron site are spin-polarized by the indirect exchange mediated by the electronic charge in excess. These small magnetic polarons are responsible for the interplay between electronic and magnetic properties that are quantitatively and self-consistently analyzed.

1. Introduction

$LiFePO_4$ is now commercialized as the active cathode element of a new generation of lithium-ion batteries. This material was already recognized as a very promising material for that purpose about 10 years ago[1] because it is low cost, nontoxic, and has a remarkable thermal stability. The main reason why it took so many years to switch from research to development of this product is its low intrinsic electronic conductivity. One way to overcome this problem was to add carbon, either by use of carbon additives to the $LiFePO_4$ matrix[1−2] or by surface coating the $LiFePO_4$ particles with thin layers of carbon.[3−6] A lot of effort has been devoted to optimizing the choice of the carbon additive to the precursors in the synthesis process for that purpose.[7−9] Other attempts to improve the electronic conductivity include addition of dispersed metal powders[10] and doping.[11] In particular, the report by Chung et al.[11] raised considerable interest and controversy by claiming that low-level doping by a range of aliovalent ions (Mg^{2+}, Al^{3+}, Ti^{4+}, Zr^{4+}, Nb^{5+}) increased the electronic conductivity by a factor of 1×10^8. There is, however, much debate concerning their defect chemistry not only because the site occupancy (Li^+ vs Fe^{2+}) is unknown but also because it is not clear whether the increase in the electronic conductivity is actually a doping effect or is simply due to a carbon coating coming from carbon-containing precursors[12] or the formation of a nanonetwork of metal-rich phosphides.[13]

This doubt has been sustained by the uncertainty in the intrinsic electronic properties of the material. For instance, the values reported for the intrinsic value of the activation energy E_a of the electronic conductivity of $LiFePO_4$ are spread over a wide range, extending from 156 meV[14] to 186 eV[15] and anywhere between 390 and 630 meV.[11,16,17] Before the effect of aliovalent ions can be addressed, we found it

* Corresponding author. E-mail: mauger@ccr.jussieu.fr.
[†] Institut de Recherches d'Hydro-Québec.
[‡] Université Pierre et Marie Curie.
[§] The University of Texas at Austin.
[||] Institut des Nano-Sciences de Paris.

(1) Padhi, A. K.; Nanjundaswamy, K. S.; Goodenough, J. B. *J. Electrochem. Soc.* **1997**, *144*, 1188.
(2) Huang, H.; Yin, S. C.; Nazar, L. F. *Electrochem. Solid-State Lett.* **2001**, *4*, A170.
(3) Zaghib, K.; Striebel, K.; Guerfi, A.; Shim, J.; Armand, M.; Gauthier, M. *Electrochim. Acta* **2004**, *50*, 263.
(4) Ravet, N.; Goodenough, J. B.; Besner, S.; Simoneau, M.; Hovington, P.; Armand, M.; *Electrochem. Soc. Meet. Abstr.* **1999**, *196*, 127.
(5) Ravet, N.; Chouinard, Y.; Magnan, J. F.; Besner, S.; Gauthier, M.; Armand, M. *J. Power Sources* **2001**, *97*, 503.
(6) Bewlay, S. L.; Konstantinov, K.; Wang, G. X.; Dou, S. X.; Liu, H. K. *Mater. Lett.* **2004**, *58*, 1788.
(7) Hsu, K. F.; Tsay, S. Y.; Hwang, B. J. *J. Mater. Chem.* **2004**, *14*, 2690.
(8) Doeff, M. M.; Hu, Y.; McLarnon, F.; Kostecki, R. *Electrochem. Solid-State Lett.* **2003**, *6*, A207.
(9) Wilcox, J. D.; Doeff, M. *Electrochem. Soc. Meet. Abstr.* **2006**, *210*, 230.
(10) Croce, F.; d'Epifagno, A.; Hassoun, J.; Deptula, A.; Olczac, T.; Scrosati, B. *Electrochem. Solid-State Lett.* **2002**, *5*, 147.
(11) Chung, S. Y.; Bloking, J. T.; Chiang, Y. M. *Nat. Mater.* **2002**, *1*, 123.
(12) Ravet, N.; Abouimrane, A.; Armand, M. *Nat. Mater.* **2003**, *2*, 702.
(13) Herle, P. S.; Ellis, B.; Coombs, N.; Nazar, L. F. *Nat. Mater.* **2004**, *3*, 147.
(14) Takahashi, M.; Tobishima, S.; Takei, K.; Sakurai, Y. *Solid State Ionics* **2002**, *148*, 283.
(15) Shi, S. Q.; Liu, L. J.; Ouyang, C. Y.; Wang, D. S.; Wang, Z. X.; Chen, L. Q.; Huang, X. J. *Phys. Rev. B* **2003**, *68*, 195108.

10.1021/cm0710296 CCC: $37.00
Published on Web 06/28/2007

desirable to clarify the origin of the electronic properties in their absence and in relation to the electronic structure of the material. Because the mobile electrons in $LiFePO_4$ occupy a magnetic Fe^{2+}/Fe^{3+} redox couple, the overall understanding of the role played by the charge carrier requires a self-consistent description of both the electronic transport properties and the magnetic properties. One also has to add the description of optical properties that probe the electronic structure. The paper is organized according to these requirements. Section 2 is devoted to the preparation of the samples used in the experiments. In Section 3, the electronic structure is analyzed in the light of previously published results of calculations that take into account the coulomb correlation of the d-electrons on the iron ions and in relation to the optical properties that we have investigated in the vicinity of the energy gap. The electronic transport is then investigated in Section 4. As a result, the strong local distortion of the lattice induced by a charge carrier is shown to be responsible for both the frequency dependence of the optical absorbance in the vicinity of the optical gap and the formation of a small polaron. The exchange mediated by the charged carrier spin-polarizes the iron ions inside the electronic orbital of the small polaron, which results in the formation of a small magnetic polaron; this polaron is studied in section 5, together with the related magnetic properties. A self-consistent description of the optical, electronic, and magnetic properties is achieved for a small polaron concentration corresponding to a fraction of trivalent iron ions $[Fe^{3+}]/[Fe^{3+}+Fe^{2+}] = 3 \times 10^{-3}$.

These results show that the material is much more ionic than the delithiated phase $FePO_4$, which is also investigated in the present work. As a result, we argue that the combination of strong ionicity of $LiFePO_4$ plus the strong bonding in the $(PO_4)^{3-}$ phosphate anions implies that aliovalent doping once envisioned to improve the electronic conductivity is impossible.

2. Experimental Section

$LiFePO_4$ specimens were prepared by the ceramic route in a laboratory rotary kiln. Stoichiometric amounts of precursors $FePO_4$-$(H_2O)_2$ and Li_2CO_3 were thoroughly mixed together after the iron phosphate had been jet-milled. Two types of samples were prepared according to the jet-milling duration; they were characterized by the quasi-monodisperse distribution of particle sizes centered at 2 and 15 μm, respectively. Carbon-free samples were obtained by heating the blend at 700 °C under a reducing atmosphere after drying. Carbon-coated $LiFePO_4$ grown from the cellulose route was prepared in solution in acetone, as reported in ref 5. The initial quantity of cellulose acetate (5 wt %) corresponded to ca. 1.2 wt % carbon on coated $LiFePO_4$ samples. After being dried, the mixture was heated at 700 °C under an argon flow. Note that the choice of this moderate sintering temperature minimizes the amount of Fe^{3+} ions in the powder, and the absence of any impurity phase has been checked by measurements of both magnetization and magnetic susceptibility. These materials were delithiated chemically by use of potassium persulfate ($K_2S_2O_8$) in an aqueous solution to form Li_xFePO_4 phases. The molar ratio of $LiFePO_4$:$K_2S_2O_8$ was 2:1 for the $x = 0$ sample. The mixture $LiFePO_4$ and $K_2S_2O_8$ dissolved in water was stirred at room temperature for 24 h. The powders were washed, filtered, and dried at 600 °C. The Li concentration was verified by ICP and XRD measurements. Both methods gave the same values.

Diffuse reflectance measurements were carried out on sintered $LiFePO_4$ pellets over the wavelength 190−700 nm (6.5−1.8 eV) with a UV−vis spectrometer (Varian, model Cary 5) equipped with an integrating sphere accessory (Specac model Selector).

Electrical conductivity measurements were carried out on pellets (0.5 mm thick, 10 mm diameter) of $LiFePO_4$ powders pressed at about 0.2 GPa and sintered at 500 °C under inert ambient atmosphere. The dc conductivity was measured with the four-probe technique and contacts were made with silver paint that are blocking for lithium. Data were collected in the temperature range 25−300 °C in a one-zone furnace. The sample temperature was kept constant within ±1 °C during a measurement.

3. Results and Discussion

3.1. Electronic Structure and Optical Properties. The several ab initio calculations of the electronic structure of $LiFePO_4$ made before 2005 have in common the use of standard density functional theory (DFT) in either the local density approximation (LDA) or the generalized gradient approximation (GGA). A review of these works can be found in the literature.[18] However, these LDA/GGA methods are unable to capture the coulomb correlation effects that are important for the d-electrons of the transition-metal elements; therefore, they predict that $LiFePO_4$ is a semimetal with no gap at the Fermi level, in obvious contradiction with the experiments that show it is insulating. Zhou et al.[18,19] have made a definitive step in the determination and understanding of the electronic structure of the compound by using the DFT + U method that is appropriate for these highly correlated electron systems. The concept is to treat the localized d-states by the Hubbard Hamiltonian while retaining the DFT Hamiltonian (LDA or GGA) for the other more delocalized states. The results of GGA + U calculations show outstanding agreement with experiments for the Li intercalation potential,[19] lattice parameters,[19] and energy gap.[18] Note that the onsite coulomb term U and the exchange term can be grouped together into a single effective parameter $U_{eff} = U - J$, so that it is actually this parameter that is the effective U parameter determined in the calculations. The value relevant to $LiFePO_4$ is $U_{eff} = 4.3$ eV.[18,19] This value is also quite consistent with the value $U_{eff} = 4.5$ eV determined by a similar ab initio calculation in the related Fe_2SiO_4 system.[20] The corresponding total density of states for $LiFePO_4$ and delithiated $FePO_4$ are reported in Figure 1 for discussion in the next section.

Figure 2 shows the diffuse reflectance spectrum of a sintered pellet sample of $LiFePO_4$ sample over the wavelength 190−700 nm (6.5−1.8 eV) at room temperature. The

(16) Delacourt, C.; Laffont, L.; Bouchet, R.; Wurm, C.; Leriche, J. B.; Morcette, M.; Tarascon, J. M.; Masquelier, C. *J. Electrochem. Soc.* **2005**, *152*, A913.
(17) Xu, Y. N.; Chung, S. Y.; Bloking, J. T.; Chiang, Y. M.; Ching, W. Y. *Electrochem. Solid-State Lett.* **2004**, *7*, A131.
(18) Zhou, F.; Kang, K.; Maxisch, T.; Ceder, G.; Morgan, D. *Solid State Commun.* **2004**, *132*, 181.
(19) Zhou, F.; Cococcioni, M.; Kang, K.; Ceder, G. *Electrochem. Commun.* **2004**, *6*, 1144.
(20) Cococccioni, M.; Dal Corso, A.; de Giroconli, S. *Phys. Rev. B* **2003**, *68*, 165107.

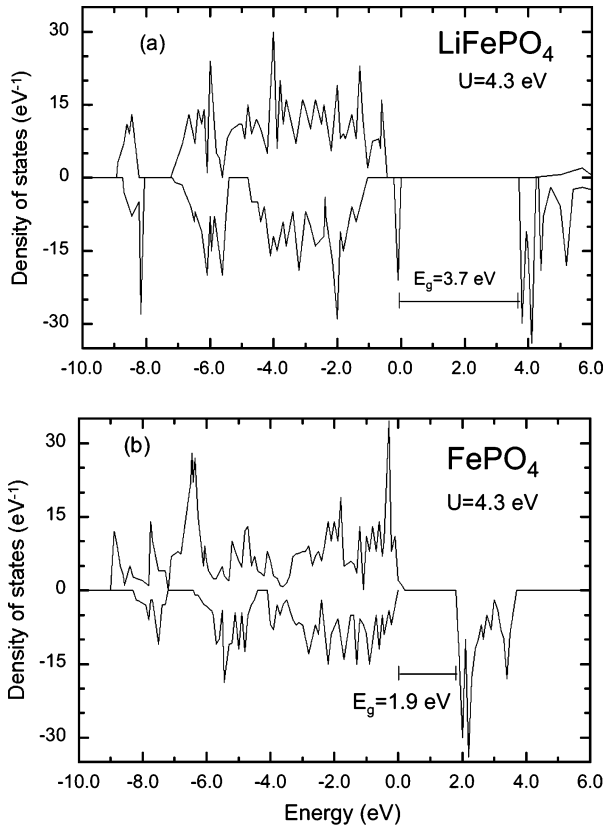

Figure 1. Total density of electronic states calculated in GGA + U for $LiFePO_4$ (a) and delithiated $FePO_4$ (b) after ref 19.

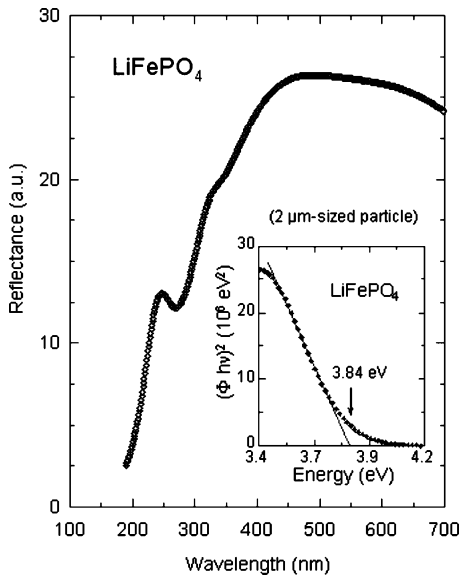

Figure 2. Diffuse reflectance spectrum of a sintered pellet sample over the wavelength 190−700 nm (6.5−1.8 eV). Insert shows the determination of the band gap of $LiFePO_4$ using the Kubelka−Munk function $\Phi = (1 - R)^2/2R$ of the diffuse reflectance spectrum. The insert shows the extrapolation $(\Phi h\nu)^2$ vs $h\nu$ to the energy axis.

reflectance rising above 250 nm is typical of the absorption threshold across the band gap. The Kubelka−Munk (KM) function, $\Phi(R) = (1 - R)^2/(2R)$, allows the optical absorbance of a sample to be approximated from its diffuse reflectance.[21] The optical band gap is determined from the KM formalism for diffuse reflectance R by extrapolating $\Phi(R)$ to the zero-energy axis. For a semiconductor, the Tauc plot $(\Phi(R)h\nu)^n$ vs photon energy will show a linear region just above the optical absorption edge for $n = 1/2$ if the band gap is direct, or $n = 2$ if the energy gap is indirect.[22] Extrapolation of this line to the photon energy axis yields the semiconductor band gap that is a key indicator of its light-harvesting efficiency under solar illumination. Figure 2 shows that Φ starts to increase linearly above 4.0 eV, in agreement with prior results.[18] In addition, we find that the Tauc plot shows a linear behavior (illustrated in the insert of Figure 2) for $n = 2$ only, evidence that $LiFePO_4$ has the characteristic behavior of an indirect gap semiconductor. The extrapolation of the line in the Tauc plot gives $E_g = 3.84$ eV for the gap of $LiFePO_4$. In addition, we find a structure in the reflectivity spectrum that goes to a secondary maximum at the wavelength 250 nm, i.e., at an energy higher than E_g.

At any Fe^{2+} ion in an oxide, the electronic states at the bottom of the energy gap must be predominantly *d*-states of the metal. The reason is that the material can be considered as ionic, so that the Madelung energy raises the Fe^{+3}/Fe^{+2} redox energy above the O^-/O^{2-} energy to stabilize the valence states Fe^{+2} and the O^{2-}, implying that the p-band of oxygen is full. Upon formation of the crystal, the p-band of oxygen is broadened by overlapping of orbitals, and the d-states associated with Fe^{+2} are localized. However, in $LiFePO_4$, the majority-spin manifold is pinned at the top of the O^{2-}:$2p^6$ band. This is confirmed by GGA + U calculations. Only the total density of states has been reported in Figure 1a, taken from ref 18. However, we can distinguish between d- and p-states by the spin polarization because the calculations have been done assuming that the material is ferromagnetic (for convenience, although $LiFePO_4$ orders antiferromagnetically at 52 K). Indeed, we can see in Figure 1a that the top of the valence band is occupied by electrons that are spin-polarized in the minority spin direction (say ↓). We can understand this result if we remember that the Fe^{2+} is in the high spin state $S = 2$, so that the d^6 multielectronic state is in the configuration $t_g^4e_g^2$, meaning 5 *d*-electrons are spin-polarized ↑ and one t_g electron is spin-polarized ↓. It is this last t_g↓ d-electron that is at the top of the valence band in the GGA + U calculation. The bottom of the conduction band in Figure 1a is also made of *d*-electrons spin-polarized in the minority spin direction, because these states lie below the bottom of the 4s band. Removal of the minority-spin d-electron from an Fe^{2+} ion leaves the Fe^{3+} ion with a multielectron majority-spin state $(t_g\uparrow)^3(e_g\uparrow)^2$ below the top of the valence band and an energy gap $E_g = 1.9$ eV to the bottom of the conduction band formed by the t_g↓ electron state. Although the U_{eff} between the high-spin d^5 and d^6 configurations is normally larger than the *U* gap between the d^6 and d^7 level, which is 3.7 eV in Figure 1a, a calculated $E_g = 1.9$ eV in Figure 1b reflects the pinning of the majority-spin state near the top of the O-2p bands, as is discussed further below.

The exponent $n = 2$ in the Tauc plot of the inset of Figure 2 reflects the small-polaron character of the excited electron−

(21) See, for instance: Kortum, G. *Reflectance Spectroscopy*; Springer-Verlag: New York, 1969.

(22) Tauc, R.; Grigorovici, R.; Vancu, A. *Phys. Status Solidi* **1966**, *15*, 627.

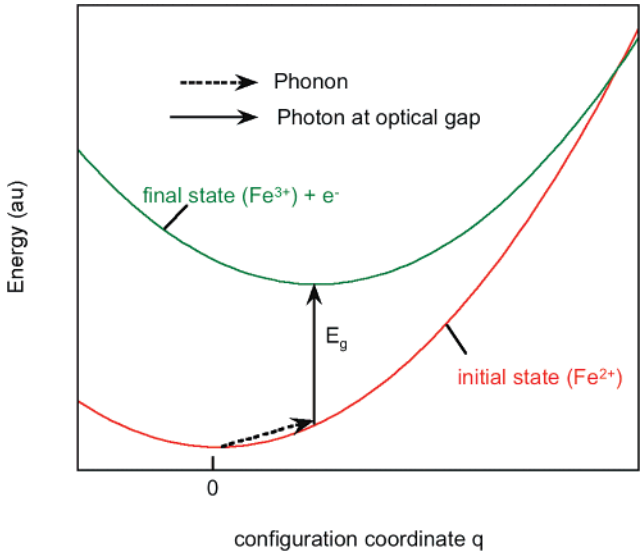

Figure 3. Configuration-coordinate diagram for electronic excitation across the energy gap of $LiFePO_4$. This Franck−Condon diagram illustrates the phonon-assisted $Fe^{2+} \rightarrow Fe^{3+}$ intra-atomic transition at the origin of the optical gap, allowing for the local distortion of the lattice upon changing the charge on a Fe site. Vertical (full) arrow represents the optical transition; the nonvertical (broken) arrow represents the phonon assistance at the origin of the "$n = 2$" behavior of the Tauc plot in the insert of Figure 2.

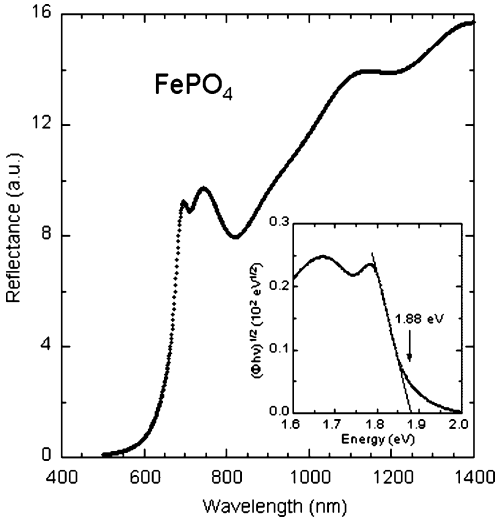

Figure 4. Diffuse reflectance spectrum of $FePO_4$ obtained by the chemical delithiation of the triphylite phase. The insert shows the plot $(\Phi h\nu)^{1/2}$ as a function of the photon energy, giving a band gap 1.88 eV.

hole pair. The minority spin states at the top of the Fe^{2+} valence band occupy a narrow energy band, and excitation of an electron from the Fe^{2+} ion leaves a smaller Fe^{3+} ion. A weak dielectric constant[23] prevents efficient screening of the crystalline charge at an Fe^{3+}, and the strong local electric field attracts the neighboring O^{2-} ions to form shorter $Fe^{3+}-O^{2-}$ bonds at a small-polaron hole. This local deformation of the lattice can be described in terms of a configurational coordinate q that shifts from $q_1 = 0$ to q_2 after relaxation of the lattice when the ionic state of the iron ion under consideration changes from Fe^{2+} to Fe^{3+}.[24] In the Franck−Condon diagram of Figure 3 illustrating the deformation energy as a function of q for both the two iron−ion states, the optical transition is "vertical", so the minimum photon energy that measures the optical energy gap E_g requires the assistance of a phonon to adjust the difference $q_2 - q_1$. The situation is thus formally identical with that of a classical semiconductor with indirect energy gap in which the top of the valence band and the bottom of the conduction band would be at wave vectors q_1 and q_2, hence the exponent $n = 2$ in the Tauc plot.

Figure 4 shows the diffuse reflectance spectrum of the chemically delithiated $FePO_4$ sample in the heterosite phase (*Pnma* symmetry). The Tauc plot now shows a linear behavior for $n = 1/2$. The energy gap is $E_g = 1.88$ eV. Again, this value is in very good agreement with the GGA + U calculation[18] also reported in Figure 1b. Note that this figure shows the top of the valence band of $FePO_4$ is not spin-polarized, which means that the electron states at the top of the valence band are now primarily p-states of oxygen. This is actually expected, because all the iron is now in the Fe^{3+} state. On the other hand, the electronic states at the bottom of the conduction band are spin-polarized in the ↓ direction, which means that they are $t_g\downarrow$ states. With a small E_g for electron transfer from O^{2-} to Fe^{3+} ions, the Fe−O bond is now more covalent. As a result, the density of states at the top of the valence band is dominantly made of p-states, but it includes a nonvanishing partial density of d-states. The bottom of the conduction band will also include a nonvanishing partial density of p states. The more covalent bonding is also evidenced by the much smaller energy gap, coming from the fact that the excitation from the occupied to the empty states is no longer a quasi-intra-atomic transition between d^5 and d^6 configurations, but a transition that is mainly between oxygen and iron states, so that it does not cost in energy the coulomb correlation potential U_{eff}. The first consequence is that this transfer of charge does not require a local distortion of the lattice and therefore does not require phonon assistance, hence $n = 1/2$ in the Tauc plot of Figure 4.

3.2. Electronic Conductivity. Figure 5 shows the electrical conductivity of carbon-coated and carbon-free $LiFePO_4$ samples. Measurements of the electronic conductivity have been made on two carbon-free pellets sintered at 500 °C with different sizes of the primary particles (2 and 15 μm). The pellet made from particles of small size had a conductivity that is 1 order of magnitude larger than the pellet formed from larger particles because of the larger number of grain boundaries. However, the activation energy is about the same: $E_a = 0.65 \pm 0.05$ eV, which is then the intrinsic property of $LiFePO_4$.

This result is in agreement with some prior experiments,[16] but it disagrees with others, because we have already pointed out in the introduction that the values reported for the intrinsic value of E_a are spread over a wide range extending from 156 to 630 meV. This uncertainty may come from different experimental set-ups, but probably it is mainly due to impurity effects. An extreme situation is met in which a carbon additive has been added to the precursors in the synthesis on purpose to improve the electronic conductivity. The carbon coating of the $LiFePO_4$ then results in an increase in the electrical conductivity by 6 orders of magnitude, as is

(23) Islam, M. S.; Driscoll, D. J.; Fisher, C. A. J.; Slater, P. *Chem. Mater.* **2005**, *17*, 5085.
(24) Maxisch, T.; Zhou, F.; Ceder, G. *Phys. Rev. B* **2006**, *73*, 104301.

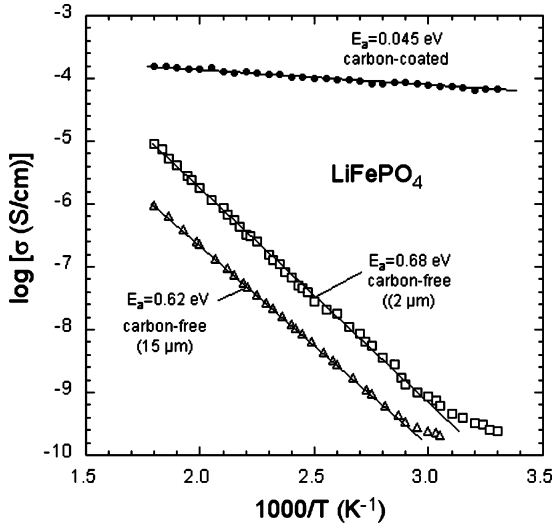

Figure 5. Arrhenius plots of the electrical conductivity of $LiFePO_4$ materials. Samples are carbon-free with grain size 15 μm (a), carbon-free with grain size 2 μm (b), and carbon-coated (c).

illustrated in Figure 5; it is associated with a huge decrease in the activation energy from 0.62 to 0.045 eV. An Fe_2P impurity phase at the particle surface also leads to a decrease of the activation energy because Fe_2P is a metal. In samples containing a few percent Fe_2P, the activation energy is almost vanishing[25,26] because the Fe_2P can then form a percolating "nanonetwork".[13] However, depending on the synthesis process, this impurity phase can also be present in a form of Fe_2P nanoparticles in a concentration too small to be detectable by X-ray analysis, but large enough to be detected by magnetic measurements.[27] In that case, the electronic conductivity will show an intermediate behavior. We then consider that the spurious presence of an impurity phase in the form of metallic nanoparticles and/or coatings are responsible for values of E_a smaller than 0.6 eV found in the literature. Another source of a spurious decrease in E_a is a nonoptimized coating of the $LiFePO_4$ particles by carbon, because the electronic conductivity and covering of the carbon deposit depends very much on the conditions of preparation of the samples.[28,29]

Because we have checked by the characterization processes described elsewhere[27,30] that the carbon-free samples we have used for the experiments are also free from any impurity phase, we consider that the intrinsic value of the activation energy for the electronic conductivity is definitively $E_a = 0.65 \pm 0.05$ eV.

This value of E_a can be compared with the activation energy of the electronic conductivity of iron phosphate glasses that have been extensively studied for more than three decades. The electronic conductivity of these glasses is the archetype of small-polaron hopping[31] that also results from the transfer of an electron from Fe^{2+} to Fe^{3+} as in $LiFePO_4$. The remarkable feature of all these iron phosphate glasses is that E_a is about the same as in $LiFePO_4$. For instance, $E_a = 0.61 \pm 0.03$ eV in binary iron phosphate $xP_2O_5 - (1-x)FeO$, for any x in the range 40−55 mol % investigated.[32] The value $E_a = 0.65 \pm 0.05$ eV relevant to $LiFePO_4$ also applies to $(50-x)FeO - 50P_2O_5 - xBaO$ in the range of composition that has been explored (10 mol % $\leq x \leq$ 35 mol %),[31] and where the modifier BaO is replaced by CaO or Na_2O.[32] We can then conclude that this value of E_a is a property characteristic of the Fe^{2+}/Fe^{3+} redox couple in a phosphate, which entirely determines the ability of the small-polaron to hop to a neighboring site. We then regard the intrinsic value of E_a we have measured as a proof that the electronic transport is a small-polaron process. Indeed, the name "polaron" comes from the fact that self-trapping of an excess-carrier is usually met in a crystalline "polar" (i.e., ionic) lattice; as we have seen, the bonding in $LiFePO_4$ is essentially ionic. σ can then be described by the general formula proposed by Mott[33,34]

$$\sigma = c(c-1)\frac{e^2\nu_e}{RkT}\exp(-2\alpha R)\exp\left(-\frac{E_a}{kT}\right) \qquad (1)$$

The rate of the wave function decay for iron ion is $\alpha = 1.5$ Å^{-1}. The distance between two neighboring Fe ions in $LiFePO_4$ is $R = 3.87$ Å. The attempt electronic frequency is $\nu_e = 1 \times 10^{15}$ Hz.[31−32] c is the ratio of the concentration $[Fe^{3+}]$ of Fe^{3+} ions over the total amount of iron ions in the matrix, $c = [Fe^{3+}]/[Fe^{2+}+Fe^{3+}]$. The fit of the experimental data in Figure 5 for the carbon-free sample with $E_a = 0.62$ eV by eq 1 is obtained for $c = 3.5 \times 10^{-3}$.

3.3. Small Polarons in $LiFePO_4$. The relevance of the small-polaron model to describe the electronic conductivity has been questioned in the recent past because the dispersion of the experimental values of E_a allowed for different models depending on which value was considered the "real" one. The determination of this parameter here removes this ambiguity. Note that E_a is actually the order of magnitude of the theoretical value for the activation energy that is expected for the ionic conductivity, i.e., for Li^+-ion transport. This feature raised the possibility that the measured conductivity is the ionic conductivity rather than the electronic one.[23] We can rule out this hypothesis here because we have made measurements of the dc conductivity with experimental conditions in which the electrodes are blocking for the lithium. Therefore, the dc conductivity σ to which we have access is purely electronic: it is the result of the small-polaron hopping as in any iron phosphate glass with the same activation energy. The only difference between iron phosphate glasses above-mentioned and iron phosphate crystals such as $LiFePO_4$ is that in glasses the concentration c can be large (typically $c \approx 0.5$) because in principle, every site can form a polaron, whereas in the crystal, one first needs a

(25) Kim, C. W.; Park, J. S.; Lee, K. S. *J. Power Sources* **2006**, *163*, 144.
(26) Xu, Y.; Lu, Y.; Yan, L.; Yang, Z.; Yang, R. *J. Power Sources* **2006**, *160*, 570.
(27) Ait-Salah, A.; Mauger, A.; Julien, C. M.; Gendron, F. *Mater. Sci. Eng., B* **2006**, *129*, 232.
(28) Julien, C. M.; Zaghib, K.; Mauger, A.; Massot, M.; Ait-Salah, A.; Selmane, M.; Gendron, F. *J. Appl. Phys.* **2006**, *100*, 1.
(29) Wilcox, J. W.; Doeff, M. M.; Marcinek, M.; Kostecki, R. *J. Electrochem. Soc.* **2007**, *154*, A389.
(30) Mauger, A.; Ait-Salah, A.; Gendron, F.; Massot, M.; Zaghib, K.; Julien, C. M. *ECS Trans.* **2007**, *3*, 115.
(31) Murawski, L. *J. Mater. Sci.* **1982**, *17*, 2155.
(32) Murawski, L.; Barczynski, R. J.; Samatowicz, D. *Solid State Ionics* **2003**, *157*, 293 and references therein.
(33) Mott, N. F. *J. Non-Cryst. Solids* **1968**, *1*, 1.
(34) Austin, I. G.; Mott, N. F. *Adv. Phys.* **1969**, *18*, 41.

defect in the lattice to introduce a carrier (hole in our case) in excess so that c is much smaller.

The transport properties do not give any information on the origin of the defects that generate the Fe^{3+} ions in $LiFePO_4$. The most probable defect in this material is the anti-site defect involving one Li^+ (radius 0.74 Å) and one Fe^{2+} (radius 0.78 Å) interchanged between two nonequivalent M1 and M2 octahedral sites. From a theoretical point of view, the Li−Fe anti-site pair is the defect that has the smallest energy.[23] From an experimental point of view, the occupancy of Li sites by Fe has been observed in the early stage of the hydrothermal synthesis of the material, in concentrations that can reach 7% if the sintering temperature is too small (i.e., below 200 °C).[35] This amount of disorder in the cation sublattice has also been found to prevent magnetic ordering in the antiferromagnetic phase at low temperature in samples prepared by the solid-state reaction below 400 °C.[36] However, this defect does not generate Fe^{3+} ions. Li on a Fe site, or more probably, a Li vacancy is the defect responsible for generating Fe^{3+} ions. An additional argument is provided by a recent work on polaron hopping in the solid solution Li_xFePO_4 ($x = 0.25, 0.55, 0.75$) formed at high temperature,[37] showing that the onset of rapid small-polaron hopping is correlated with the temperature at which the lithium ions begin to disorder in the lattice, so that the two events are correlated. The large value of the activation energy has been previously discussed in terms of the coupling effect to form an excitonic electron−Li^+ pair.[24,37] However, the small-polaron should not be this excitonic pair for two reasons. First, this pair is neutral in terms of electronic charge, so that it does not generate an electronic current. In addition, we have shown here that this activation energy is a common feature to all iron phosphate glasses that do not have any lithium in their composition. The link between lithium and a small polaron should then be restricted to the fact that the Li vacancies are a reservoir of Fe^{3+} ions. The $t_g\downarrow$ electron is bound to the Li^+ vacancy by the coulomb potential, but this pair can be broken by the application of the electric field, hence the electronic current generated by the hopping of the $t_g\downarrow$ electron.

3.4. Magnetic Polaron Effects. In the paramagnetic configuration, the majority-spin direction has to be taken in the Hartree−Fock sense, i.e., as the direction of the local magnetic moment carried by one iron ion resulting from the uncompensated moment of the electrons that occupy the 3d-shell of the ion under consideration. Therefore, the $t_g\downarrow$ electron of one Fe^{2+} ion on site i is spin-polarized in the direction opposite to the local spin $\vec{S}_i$ carried by the iron ion on site i. In a hopping process, this electron jumps by the tunneling effect on the nearest-neighboring (nn) Fe^{3+} ion on site j in the initial state $(t_g\uparrow)^3(e_g\uparrow)^2$ to make it Fe^{2+} in the final state is $(t_g\uparrow)^3(e_g\uparrow)^2t_g\downarrow$. But in this final state, the spin polarization refers to the direction of the spin $\vec{S}_j$ carried by the iron on site j. This hopping, illustrated in Figure 6a, is

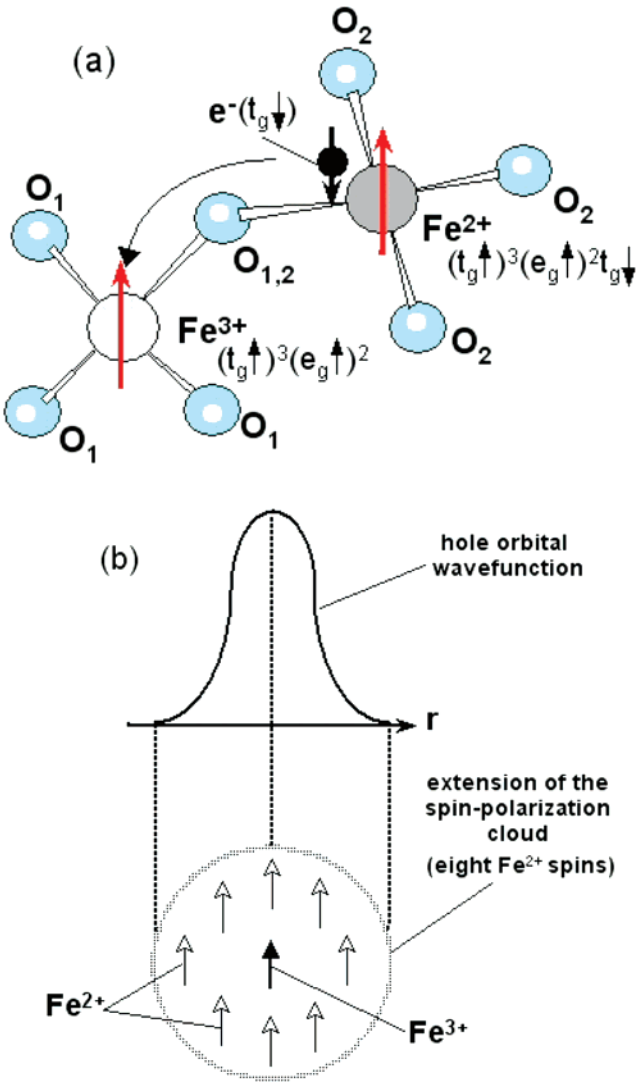

Figure 6. Small magnetic polaron in $LiFePO_4$. The hopping process is illustrated in (a). The $t_g\downarrow$ "hole" on the Fe^{3+} site 1 is shifted to a neighboring iron site 2 by transfer of one $t_g\downarrow$ electron from site 2 to site 1. The indirect exchange interaction is responsible for the spin-polarization of the iron ions inside the electronic $t_g\downarrow$ "hole" wavefunction (in the direction opposite to that of the t_g electron), as it is illustrated in (b). As the charge in excess hops from site to site, it brings with it not only a local lattice deformation cloud associated with the Coulomb potential but also its spin-polarization cloud.

thus possible only if both iron ions on site i and j are spin-polarized in the same direction because of the Pauli principle. Therefore, there is a direct antiferromagnetic interaction between the $t_g\downarrow$ (hole) centered on the Fe^{3+} ion i and all the spins inside the $t_g\downarrow$ (hole) orbital, imposed by the Hund's rule. This direct exchange is responsible for a ferromagnetic ordering of the iron spins inside the polaron in the opposite (↑) direction. The result is that the moving electron must carry with it not only its distortion cloud, but also its spin-polarization cloud, as shown in Figure 6b. The small polaron is then also a so-called "magnetic polaron" that has been extensively studied in the past, in rare earth oxides,[38] or in diluted magnetic semiconductors.[39] In these earlier works, we had also envisioned the case of an extra charge that digs

(35) Chen, J.; Whittingham, M. S. *Electrochem. Commun.* **2006**, *8*, 855.
(36) Ravet, N.; Gauthier, M.; Zaghib, K.; Goodenough, J. B.; Mauger, A.; Gendron, F.; Julien, C. M. *Chem. Mater.* **2007**, *19*, 2595.
(37) Ellis, B.; Perry, L. K.; Ryan, D. H.; Nazar, L. F. *J. Am. Chem. Soc.* **2006**, *128*, 11416.
(38) For a review on magnetic polarons, see: Mauger, A.; Godart, C. *Phys. Rep.* **1986**, *141*, 51.
(39) Scalbert, D.; Gaj, J.; Mauger, A.; Cernogora, J.; Benoit à la Guillaume, C. *Phys. Rev. Lett.* **1989**, *62*, 2865.

its own exchange potential well so that its orbital self-localized, without the need of coulomb interaction. This kind of magnetic polaron is a quasiparticle also sometimes called a ferron.[38] More often, the magnetic polaron is bound to a donor (or acceptor) because of the coulomb attractive potential, and the indirect exchange mechanism only contributes to shrink the orbital of the excess electron (hole). This is the "bound magnetic polaron". There is, however, an important difference between the magnetic polaron we have investigated in the past, and the present case. Prior studies of magnetic polarons concerned nonionic materials with important magnetic exchange interactions, in which case, the magnetic polaron may have tremendous effects on electronic transport properties,[40] and the effective magnetic moment μ_{pol} carried by a magnetic polaron can be large.[41] Here, the orbital of the excess charge carrier is strongly localized by the distortion of its surroundings, because the material is ionic. The consequence is that the contribution of the magnetic exchange interaction to the shrinking of the polaron orbital[40,41] is negligible here, so that the spin-polarization process does not significantly influence the transport properties. The other consequence, closely linked to the previous one, is that the magnetic moment associated to the spin-polarization of the cloud is small, because the orbital is much more localized than in nonionic compounds so that only the neighbors of the central polaron site can be spin-polarized. A reasonable approximation amounts to take into account the neighbors that are effectively magnetically coupled to a given ion atom in the $LiFePO_4$ lattice, although the exchange mechanism we have invoked for the spin-polarization inside the magnetic polaron is a d−d direct exchange not mediated by the oxygen. The magnetic interactions in $LiFePO_4$ have been determined in the literature.[42] Keeping the same notations as in this prior work, it includes the four Fe ions coupled by the intralayer interaction J_1, two ions coupled by an interlayer super−super exchange interaction J_2, and two ions coupled by an intralayer interaction J_b. The number of neighboring Fe^{2+} ions spin−polarized by the excess carrier centered on an Fe^{3+} site should then be 8 in total. Because the spin of the central Fe^{3+} ion is $S = 5/2$ and the spin of the nn Fe^{2+} ions is $S = 2$, we expect the macrospin associated with the polaron to be $S_{pol} = 5/2 + 8 \times 2 = 18.5$, hence a magnetic moment $\mu_{pol} = gS_{pol} = 37$ in Bohr magneton unit (we take $\mu_B = 1$ throughout this work).

This moment can be detected by magnetic measurements. In the paramagnetic regime in which the Curie−Weiss law is satisfied, the Curie constant C will be the sum of the intrinsic contribution of $LiFePO_4$ plus the contribution of the polarons, namely

$$3k_B C = (1 - c)[\mu(Fe^{2+})]^2 + c(\mu_{pol})^2 - 8c[\mu(Fe^{2+})]^2 \quad (2)$$

Here, C is reported per iron ion. The last (negative) term in eq 2 comes from the fact that the contribution of the eight Fe^{2+} ions involved in a polaron have their contribution included in the second term, so that they must be subtracted from the host contribution (first term). The experimental effective moment μ_{eff} deduced from the slope of the $\chi^{-1}(T)$ curve, where $\chi = C/(T - \theta)$ is the magnetic susceptibility, is defined as

$$C = \mu_{eff}^2/(3k_B) \quad (3)$$

In carbon-free samples, the magnetic susceptibility must be defined as the slope of the magnetization curves $M(H)$, i.e., $\chi = dM/dH$ measured at $H = 10$ kG. At this large magnetic field, the superparamagnetic contribution of the impurity phases to M is saturated, so that the impurity phases, if any, do not contribute to χ.[27,30] The experimental value of μ_{eff} we have found for our samples is $\mu_{eff} = 5.3$. That is in excess with respect to the intrinsic value $\mu(Fe^{2+}) = 4.9$ expected for the pure stoichiometric sample. Reporting this value in eqs 2 and 3, for $c = 3 \times 10^{-3}$ determined from electronic transport experiments, we find $\mu_{pol} = 38$, in good agreement with the expected value. The description of the optical, electronic, and magnetic properties of $LiFePO_4$ is then fully self-consistent.

An experimental value $\mu_{eff} = 4.9$, in quantitative agreement with the theoretical value, has already been reported in the literature in different works. However, with the synthesis process described in section 2, we find μ_{eff} in the range 5.1−5.3, depending on the sample. The magnetic susceptibility associated with the carbon itself is negligible, which explains that we find the same excess in the effective magnetic moment for carbon-coated and carbon-free particles. This result, however, is nontrivial, because it gives the proof that the organic additive has no effect on the native defects associated with the formation of the polarons, although it does have a reducing power on iron. Therefore, this result gives more evidence that the native defects are not related to iron and pleads in favor of our assumption that they are Li vacancies.

Attention should also be paid to the fact that the effective spin S_{pol} is small enough so that the argument $\mu_{pol}H/(k_BT)$ of the Langevin function that determines the spin-polarization of the small polaron remains small in the whole range of the magnetic field investigated. To the contrary, the nanoparticules of impurity phases have a huge effective magnetic momentum, giving a component to the magnetization that easily saturates under the application of the magnetic field H so that their contribution to dM/dH in a large magnetic field is negligible.[27] That is the very reason why the polaron effect can be distinguished from the impurity phase effects on the magnetic properties, without any ambiguity. This is further evidence that the investigation of magnetic properties is a powerful tool to characterize this material.

3.5. Discussion on Doping Attempts. Recent calculations have determined that this material is not tolerant to aliovalent doping.[23] The present work allows us to get some insight into understanding this feature. The first reason is the ionic nature of the material evidenced in the present work. As the material is ionic, any change in the charge distribution is expensive in energy. Therefore, any trial to put divalent

(40) Mauger, A.; Godart, C. *Solid State Commun.* **1980**, *35*, 735.
(41) Mauger, A.; Mills, D. L. *Phys. Rev. B* **1985**, *31*, 8024.
(42) Dai, D.; Koo, H. J.; Rocquefelte, X.; Jobic, S. *Inorg. Chem.* **2005**, *44*, 2407.

dopants (like Mg, Mn, Co, or Ca^{2+}) on a Li site will fail, because these aliovalent elements will prefer to be located on Fe sites to ensure charge neutrality. This is indeed the result of the calculations,[23] and what is observed experimentally.[1,16] The substitution of Fe by these isovalent elements, however, does not introduce any charge carrier in excess and then does not modify the electronic conductivity. In the same way, the Fe site is more favorable than the Li site for substitution by trivalent, tetravalent, pentavalent ions, because this is again the site that minimizes the change in the charge distribution; this is because Fe is already divalent, whereas Li is monovalent. Still, the energy required for this substitution is prohibitive.[23] Interesting enough, this is a major difference with some other systems. For instance, ZrO_2 can be doped with Y_2O_3 or CaO. This is a well-known example because this doping has possible applications such as oxide fuel cells and oxygen sensors.[43,44,45] The main reason why this is possible is that the partial substitution of a lower-valent cation for the tetravalent zirconium generates oxygen vacancies, and indeed, it is part of the working principle of the oxygen sensor in the car exhaust system that feeds the controller of the car engine in order to keep emissions at the lowest possible level. This is impossible in $LiFePO_4$, simply because the bond within the $(PO_4)^{3-}$ phosphate anions is very strong and cannot be broken at reasonable energetic price to generate an oxygen vacancy. The impossibility for doping $LiFePO_4$ is then the combined effect of two features: the material is ionic, plus the P−O bond is too strong.

Of course, doping $LiFePO_4$ with pentavalent ion is even more impossible because the charge difference with iron is even larger. Recently, the combination of high-resolution microscopy Raman mapping and current-sensing atomic force microscopy has shown that the pattern of conductivity of the sample prepared with a niobium additive corresponds exactly to the pattern of the carbon distribution.[46] It is the definitive proof that the improvement in the conductivity in this case is not induced by the niobium, but by the carbon coating, the carbon coming from the fact that the niobium-containing precursor was an organic compound.

4. Concluding Remarks

In conclusion, we have achieved an overall understanding of optical, electronic, and magnetic properties of $LiFePO_4$. The optical gap of $LiFePO_4$ is related to a transition $3d^6 \rightarrow 3d^5$ of an iron ion so that E_g is related to the intra-atomic coulomb correlation potential that separates in energy multielectronic states with different occupation numbers in the 3d-shell. It is then in nature an intra-site $Fe^{2+} \rightarrow Fe^{3+}$ transition. This is at contrast with the situation met in the much more covalent $FePO_4$ material, where the band gap is associated with a transition that is intersite in nature, between a p-electron of oxygen and a d-electron on iron. In carbon-free $LiFePO_4$, the electronic conductivity occurs via the small-polaron process. In the carbon-coated sample, the electronic conduction is driven by the carbon, so that it is no longer possible to detect the small polarons by transport experiments. In this latter case, however, magnetic measurements are able to reveal their existence, because the small polaron is also a magnetic polaron that carries a magnetic moment associated with the ferromagnetic spin-polarization of the eight iron ions around the central Fe^{3+} site. This spin-polarization is due to the exchange of the t_g-hole with the localized spins of the iron ions inside the t_g-hole orbital. The localization is imposed by the electrostatic energy associated with the ionic nature of the bonds in the lattice so that the small polaron is truly a Holstein small polaron. The spin distortion is only the consequence of this localization, and the magnetic binding energy associated with it[41,47] that was responsible, for instance, for the localization of the electron orbital in europium chalcogenides[38] is negligible here. The activation energy of the electronic conductivity E_a is in agreement with the value that has been determined for all the iron phosphate glasses (0.65 ± 0.5 eV) and is then not related to the lithium. It is related to an energy barrier that an electron has to overcome in the intersite $Fe^{2+} \rightarrow Fe^{3+}$ transition (not to be confused with the intrasite transition associated with the energy gap) due to the presence of native defects generating a fraction $c = 3 \times 10^{-3}$ of iron ions in the trivalent state due to lithium vacancies. The actual chemical formula for our sample is then $Li_{1-c}FePO_4$. Note that we are in the situation in which the Li vacancies are randomly distributed, because $Li_{1-c}FePO_4$ is a solid solution for $c < 0.11$.[48]

The combination of strong ionicity of the material plus the strong bonding in the $(PO_4)^{3-}$ phosphate anions implies that aliovalent doping to improve the electronic conductivity is hopeless. This will be true for the materials that fulfill the same criteria, i.e., ionic phosphate compounds. It includes in particular $LiCoPO_4$, and indeed, a recent attempt to increase the electronic conductivity of this material by doping has failed.[49] Actually, because the aliovalent elements *M* cannot enter in the $LiFePO_4$ lattice, a large enough amount of *M*-containing additive to the precursors in the course of the synthesis may result in metallic nanoprecipitates of *M* or *M*-rich metallic nanodomains. This procedure is then identical to other attempts to improve electronic conductivity by forming a percolating nanonetwork of metallic phosphates. This is indeed a solution to improving the electronic conductivity, but it is at the expense of the ionic conductivity, so it damages the electrochemical properties.[25] Therefore, this process should be avoided. The carbon coating of the particles by using an organic carbon additive in the synthesis process is presently the way to improve the electronic conductivity without damaging the ionic conductivity.

Acknowledgment. The authors are grateful to Dr. Michel Gauthier for fruitful discussions.

CM0710296

(43) Etsell, T. H.; Flengas, S. N. *Chem. Rev.* **1970**, *70*, 339.
(44) Subbarao, E. C.; Maiti, H. S. *Solid State Ionics* **1984**, *11*, 317.
(45) Arai, H. *Bull. Ceram. Soc. Jpn.* **1992**, *27*, 100.
(46) Chen, A.; Kostecki, R. http://www.lbl.gov/Science-Articles/Archive/sabl/2007/Feb/future-batteries-II.html.
(47) Mauger, A.; Mills, D. L. *Phys. Rev. Lett.* **1984**, *53*, 1594.
(48) Yamada, A.; Koizumi, H.; Nishimura, S.-I.; Sonoyama, N.; Kanno, R.; Yonemura, M.; Nakamura, T.; Kobayashi, Y. *Nat. Mater.* **2006**, *5*, 357.
(49) Wolfenstine, J. *J. Power Sources* **2006**, *158*, 1431.